# MEASURING WAVE RUN-UP, OVERTOPPING AND DAMAGE OF RUBBLE-MOUND BREAKWATERS IN SCALE MODEL TESTS

João A. Santos (1), Rute Lemos (2), Julius Weimper (3), Oliver Gronz (3), Bas Hofland (4), José Sande (5), Liliana Pinheiro (2), Jan H. Spans (6), Enrique Peña (5), Maria Teresa Reis (2), Conceição Juana Fortes (2), Andrés Figuero (5), Emilio Laiño (5), Antje Bornschein (7), Nils B. Kerpen (8), Francisco Pedro (1), Mário Coimbra (1), Moritz Körner (7), Jeroen van den Bos (4), Bastien Dost (3), Rita Carvalho (9), Alberto Alvarellos (5) & Reinhard Pohl (7)

(1) ISEL – Instituto Superior de Engenharia de Lisboa, Instituto Politécnico de Lisboa, Portugal, E-mail: jasantos@dec.isel.ipl.pt, a32643@alunos.isel.pt, a39777@alunos.isel.pt
(2) LNEC, Portugal, E-mail: rlemos@lnec.pt, lpinheiro@lnec.pt, treis@lnec.pt, jfortes@lnec.pt
(4) UTrier, Germany, E-mail: weimper@uni-trier.de, gronz@uni-trier.de, s6jodost@uni-trier.de
(5) TU Delft, the Netherlands, E-mail: B.Hofland@tudelft.nl, J.P.vandenBos@tudelft.nl
(6) Universidade da Coruña, Spain, E-mail: jose.sande@udc.es, epena@udc.es, andres.figuero@udc.es, e.laino@udc.es, alberto.alvarellos@udc.es
(3) Saxion University of Applied Sciences, The Netherlands, E-mail: 444898@student.saxion.nl
(7) TU Dresden, Germany, E-mail: antje.bornschein@tu-dresden.de, reinhard.pohl@tu-dresden.de, koerner.moritz96@icloud.com
(8) Leibniz University Hannover, Germany, E-mail: kerpen@lufi.uni hannover.de
(8) MARE, UCoimbra, Portugal, E-mail: ritalmfc@dec.uc.pt

A set of scale-model tests was carried out at the wave basin of the Leibniz University Hannover to extend the range of wave steepness values analysed in run-up, overtopping and armour layer stability studies, focusing on oblique extreme wave conditions and on their effects on a gentler slope breakwater's trunk armour and roundhead. The paper describes the model set-up and operation concentrating on the measurement techniques used in those tests, namely on the innovative techniques for armour layer damage characterization.

## 1. INTRODUCTION

Wave breaking / run-up / overtopping and their impact on the stability of rubble-mound breakwaters (both at trunk and roundhead) are not adequately characterized yet for climate change scenarios. The same happens with the influence of high-incidence angles on such phenomena.

Several former investigations on wave run-up and overtopping of (impermeable and permeable) coastal structures aimed at quantifying the influence of oblique waves on mean overtopping discharge, water layer thickness and velocities through the development of empirical formulas of a reduction factor for wave obliquity (e.g. Nørgaard et al., 2013). However, most of the formulas did not consider very oblique wave approach.

Regarding the stability of armour layers, several authors have proposed guidelines on how to consider the effects of oblique waves (e.g. Van Gent, 2014). Especially for very oblique waves, for which the increase in stability is the largest, limited data are available.

Van Gent (2014) performed a set of physical model tests to assess the effects of oblique waves on the stability of rock slopes and of cube armoured rubble-mound breakwaters (single and double layers) mostly on a 1:1.5 slope. The tests included wave directions between perpendicular (0°) and parallel (90°) to the longitudinal structure axis, with long and short-crested waves. A series of tests was performed with an increasing wave height between 0.025 m to 0.274 m and constant wave steepness of 0.03 or 0.04 (only for a few tests).

Van Gent (2014) recommends the study of the influence of oblique wave attack on the stability of rubble-mound structures for: a) other slope angles, especially gentler rock slopes; b) other values of wave steepness, to cover values of the surf similarity parameter outside the range of 2.2-3.5 for rock and 3-3.5 for cubes; c) interlocking armour units.

The gaps in existing data and the R&D&I experience of the team members triggered the common interest in developing the present experimental work. Its main goal is to contribute to a new whole

understanding of the phenomena to mitigate the effects of future sea-level rise on European coastal structures, including the run-up and overtopping characterization on rough and permeable slopes, as well as to check and extend the validity range of the formulas developed for armour layer stability.

The key point is to expand the range of wave steepness values analysed in run-up, overtopping and armour layer stability studies, focusing on oblique extreme wave conditions and on their effects on gentler sloping breakwater's trunk armour and roundhead. By studying wave run-up and overtopping of porous armour layers, the present work covers Van Gent (2014) recommendations.

This paper aims at describing this experiment, which involved people from eight different institutions and lasted for six weeks, starting with an empty wave tank at the Marienwerder facilities of the Leibniz University Hannover (LUH) and finishing with a rubble-mound again in an empty tank. The paper includes a brief description of the model construction as well as the equipment used in the experiments, the test plan and some preliminary results.

## 2. MODEL CONSTRUCTION

A stretch of a rubble-mound breakwater (head and part of the adjoining trunk, with a slope of 1(V):2(H)) was built in the wave basin of the LUH to assess, under extreme wave conditions (wave steepness of 0.055) with different incidence wave angles (from 40º to 90º), the structure behaviour in what concerns wave run-up, wave overtopping and damage progression of the armour layer. Two types of armour elements (rock and Antifer cubes) were tested.

Fig. 1 presents the plan view of the breakwater model as well as the cross section. The trunk of the breakwater was 7.5 m long and the head had the same cross section as the exposed part of breakwater. The model was 9.0 m long, 0.82 m high and 3.0 m wide. The reason for building such a large breakwater model is to reduce the scale effects associated to wave-induced flows across small models. The angle between the longitudinal axis of the breakwater and the tank wall was 70º.

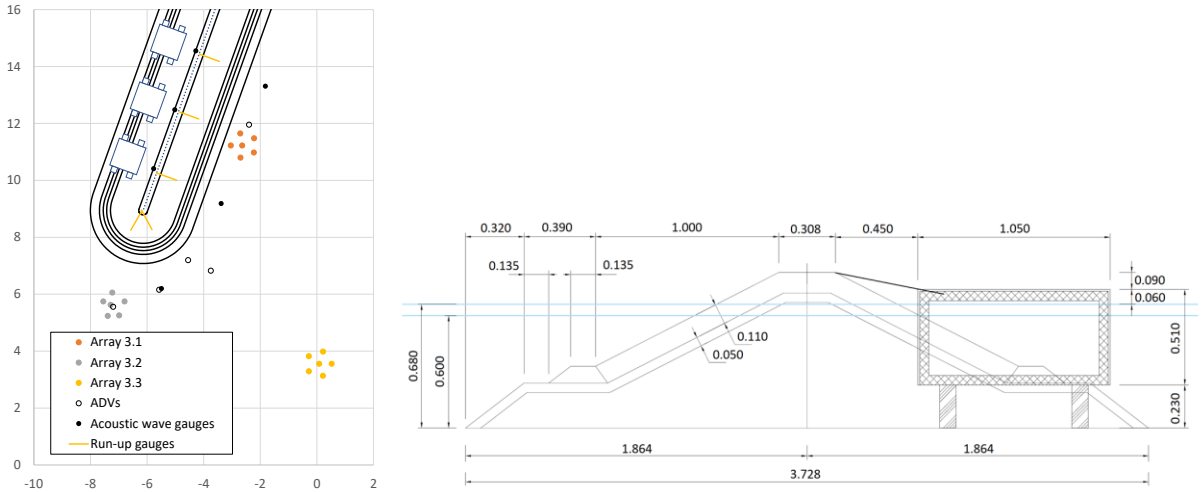


Figure 1. Plan view and cross-section of model breakwater

The model construction started with the assembly of a cage made of the core moulds for the breakwater trunk and connecting beams. Once the cage was complete, it was positioned at the wave tank bottom so that the desired alignment for the model axis was obtained. One extra mould was placed orthogonal to the end of the trunk, to help with the breakwater head construction.

Before starting to build the core by pouring the gravel (15 $m^3$ with a median weight of 6 gf), the three overtopping reservoirs were put in place. Once the core of the breakwater model was built, the moulds for the filter layer were placed on top of the core moulds and the filter layer material (gravel with a median weight of 59 gf) was poured in the remaining spaces and shaped as in the core.

After the shaping of the filter layer was complete, its moulds were removed from all trunk cross-sections. At the breakwater head, both the core and the filter layer moulds were removed to ensure nothing hampered the percolation across the core of the breakwater's head.

Then the moulds for the toe berm were placed on top of the filter layer. These moulds were held in place with small mounds of the toe material (gravel with a median weight of 260 gf) placed on both sides of each mould and then the rest of the toe was built along the breakwater.
The construction of the breakwater armour layer started at the breakwater head and at the 2.5 m wide adjoining strip. Here, 351 gf Antifer cubes were deployed in two layers, such that the porosity of the armour layer was 37%. Gravel with a median weight of 315 gf was employed both at the exposed and lee parts of the rock armour layer.

## 3. EQUIPMENT DEPLOYED

Four different categories can be identified in the equipment deployed in the experiment according to the variables measured:

- Sea waves;
- Run-up;
- Overtopping;
- Armour layer damage.

A plan view of the key instruments for those variables (apart from “armour layer damage”) is presented on the left of Fig. 1.
The sea waves generated by the wavemaker, as well as the incident sea waves on the structure and the ones reflected by it, were measured with arrays made of six acoustic wave probes (the vertices of an approximately regular pentagon and its centre of gravity). One wave gauge array was deployed in front of the wavemaker, another in front of the breakwater head, aligned with the breakwater crest, and one approximately at the middle of the breakwater trunk, in front of the entrance to the second overtopping reservoir.
In front of the entrance to the first and third overtopping reservoirs, two isolated acoustic wave probes were deployed. A third acoustic wave probe was deployed in front the breakwater head, approximately in the middle of the dihedral angle formed by the vertical plane that marks the end of the trunk and the plane that contains the middle of the breakwater crest.
Five acoustic Doppler velocimeters (ADV) were deployed close to the breakwater to characterise the wave-induced flow there. Three of them were deployed close to acoustic wave probes, to have an alternative source of information to compute the incident and reflected waves. The remaining two ADVs were placed approximately on the vertical plane that marks the end of the breakwater trunk. Despite the difference between the vertical positions of the acoustic transmitter of the several ADVs, the acoustic receiver that defines the x-axis was aligned with the breakwater crest in all ADVs.
Capacitive wave gauges, 0.87 m long, were deployed over the armour layer to measure wave run-up. Three were deployed at the breakwater trunk, close to the sections where wave overtopping was to be measured, and two at the breakwater head (one in the plane that contains the breakwater axis and the other was deployed perpendicularly to it).
A staff graduated with a chequered pattern was used close to the run-up gauge of the root overtopping reservoir, to get an alternative way of measuring run-up by processing the video frames obtained with a camera during the experiments. This staff was embedded in the armour layer and a column made of 20 black and white squares had a length of 0.328 m.
Each overtopping reservoir had a capacity of 500 l and was placed inside a watertight container. The water volume inside each overtopping reservoir was weighted with a load cell placed between the bottom of that reservoir and its container. A trapezoidal chute 0.60 m long and an entrance width of 0.60 m (and an exit width of 0.50 m) conveyed the overtopped water volume from the inner edge of the breakwater crest into the reservoir. An acoustic wave probe was deployed above the entrance of each chute to identify the occurrence of overtopping events. A capacitive wave gauge was placed inside each overtopping reservoir to have some redundancy in the measurement of the overtopping volume provided by the load cell. The cross-section in Fig. 1 includes the overtopping reservoir and the chute from the breakwater crest into the reservoir. In Fig. 3 there is a picture from the entrance of the overtopping reservoir at the breakwater root. In addition to the chute, the acoustic wave gauge to identify overtopping events and the graduated staff deployed in front of that reservoir can be seen. During the tests, a video camera recorded the free-surface on the graduated staff. It is expected that run-up parameters can be extracted from such videos using the methodology of Bornschein et al. (2014).
Three different techniques were used to measure armour layer damage in the tests, in addition to the visual identification of rocking and displaced armour units.

Figure 3. General layout at the entrance of an overtopping reservoir (run-up wave gauge, acoustic wave gauge to identify overtopping events, graduated staff).

The first one is based in stereo photogrammetry. This means that two cameras have to hang above the breakwater model so that two simultaneous pictures of almost the same area can be taken by the two cameras. The procedures implemented to process the photo pairs enable the reconstruction of the scene corresponding to the submerged part of the breakwater without the need to remove the water from the wave basin, Pedro et al. (2015).
The second technique is based on the use of the Kinect motion sensor that travels over the study area. A reconstruction of the armour layer's above-water region can be made based on the collected information. Additionally, since it is possible "to see" below the water level, a first estimate of the armour layer's submerged region can also be made. Such rough estimate can be corrected with the information gathered with the Kinect motion sensor after the water is removed from the wave tank, Sande et al. (2018).
Since these two techniques implied the movement of the measuring equipment above the study region, an aluminium rail made of a straight stretch 7.85 m long and of a semi-circumference stretch with a diameter of 1.80 m was hung 2.00 m above the wave basin bottom. Fig. 4 shows the rail assembly as well as the special wagon that was moved along the rail and where the cameras ensemble or the Kinect motion sensor were hung.
A laser scan survey of the armour layer envelope established the ground truth for the measurements made with the other techniques. This was done at the second day of tests, just before the beginning of the test series and at the end of that test series. The same happened with the last test series.

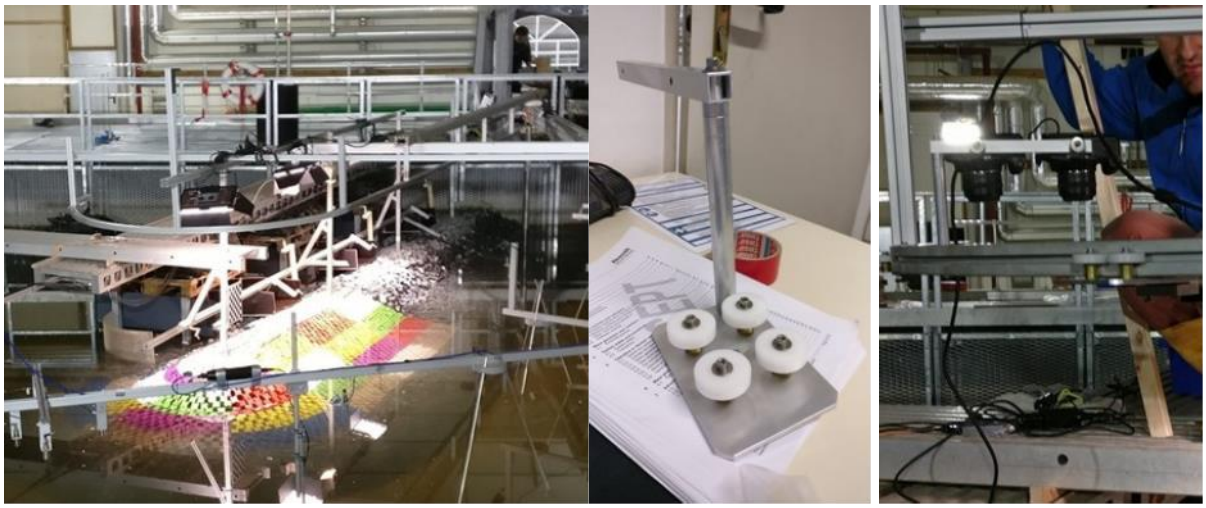

Figure 4. Left: rail to support the photographic cameras and the Kinect motion sensor; Middle: wagon to carry those cameras; Right: wagon on the rail with two cameras.

The third technique consists on the use of accelerometers inside a couple of armour layer elements, an extension of the Smartstones of Gronz et al. (2016). In these experiments 6 of such artificial armour elements were used, although there were not all working at the same time. Also, a second type was used. In these sensors open-source Arduino based hardware was used to obtain accelerations and rotations of the units (Hofland et al., 2018). These sensors were embedded in 3D-printed Antifer shapes that were weighted by lead to obtain the correct mean density. The main aim of using these sensors was to get experience in a project, to see whether this relatively cheap technology is developed enough to be used in an elaborate large-scale project like the present one. Two out of four functioned well for all tests. All smart Antifers were placed on the roundhead around the water line facing the incoming wave direction, as can be seen in Fig. 5.

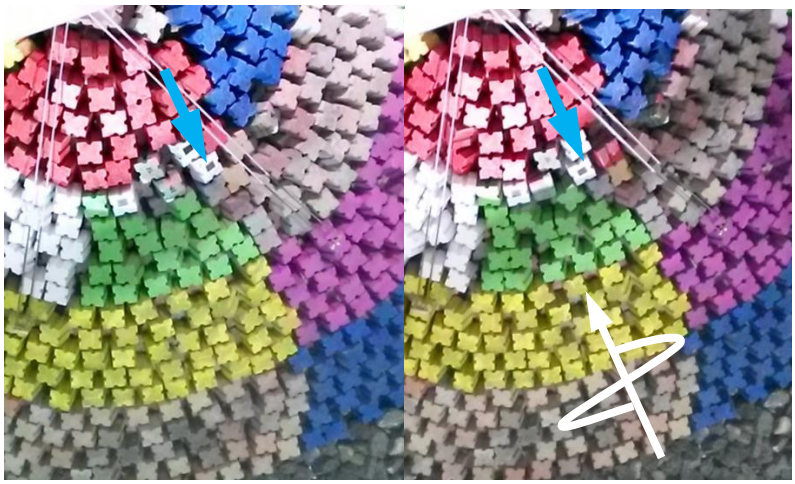

Figure 5. Three instrumented Antifer cubes in the roundhead, before (left) and after (right) test 23. Blue arrow points to the so-called “Cube 3”

Before and after each test, pictures were made from exactly the same position above the area where the smart armour units were deployed. From these picture sets small settlements can be detected (Hofland and Van Gent, 2016). These will be used to see whether the rocking of –and possible mechanical damage to– the Antifers can be linked to these small settlements.

## 4. TEST PLAN

For each incidence wave angle, at least 4 different wave conditions acted on the model (significant wave heights Hs=0.100 m, 0.150 m, 0.175 m and 0.200 m and the corresponding peak periods Tp=1.19 s, 1.45 s, 1.57 s and 1.68 s).
For long-crested waves and a water depth of 0.60 m, 5 incidence wave angles (40º, 55º, 65º, 75º and 90º) were considered. Since no major run-up, overtopping or damage were expected along the structure for high incidence angles, in the test series with a water depth of 0.68 m and long-crested waves, the number of incidence angles was reduced to 3 (40º, 55º and 65º).
The influence of the directional spreading of short-crested waves was investigated for the lowest water depth (0.60 m) and the incidence angles of 40º and 65º, the directional spreading being 50º. Finally, for the incidence angle of 40º results were also obtained for the highest water depth (0.68 m) and short-crested waves with a directional spreading of 50º.

## 5. RESULTS

Since some equipment was brought by the people from the institutions participating in the experiments and taken with them when they returned home, the first set of data chosen to be processed was for a water depth of 0.60 m and incident long-crested waves making an angle of 65º with the normal to the breakwater axis. This corresponds to a period when all equipment was available for the experiments. Moreover, for this set of experiments, it was possible to have a laser scan survey before it started and after its end.

### 5.1 Sea waves

The data collected at the acoustic arrays was processed for each array individually, using temporal and spectral analyses. Table 1 presents the averages of the significant wave heights and of the peak periods obtained for each array and test of the series.

Table 1. Wave characteristics. Average quantities obtained in the acoustic wave gauge arrays with temporal and spectral analyses.

| Test | Goal | | Array 3.3 | | Array 3.2 | | Array 3.1 | |
|---|---|---|---|---|---|---|---|---|
| | Hs (m) | Tp (s) | Hs (m) | Tp (s) | Hs (m) | Tp (s) | Hs (m) | Tp (s) |
| 17 | 0.100 | 1.19 | 0.108 | 1.19 | 0.100 | 1.19 | 0.107 | 1.19 |
| 18 | 0.150 | 1.45 | 0.147 | 1.47 | 0.143 | 1.46 | 0.150 | 1.47 |
| 19 | 0.175 | 1.57 | 0.168 | 1.58 | 0.162 | 1.60 | 0.171 | 1.57 |
| 20 | 0.200 | 1.68 | 0.189 | 1.65 | 0.177 | 1.67 | 0.185 | 1.69 |

The values for array 3.3, the one closest to the wavemaker, are quite similar to the test goal. Peak-period relative errors are smaller than 2% whereas the maximum significant wave height relative error is equal to 8% (it occurs for the smallest wave height).

The MATLAB toolbox DIWASP (Johnson, 2002) was employed to evaluate the directional spectrum of the waves at the location of the arrays made of acoustic wave probes. The six probes in each array were used to estimate the directional spectrum with the iterated maximum likelihood method of Pawka (1983). Since in this set of tests the wavemaker generated long-crested waves only, the estimated directional spectra are quite narrow, with most of the energy concentrated around the direction of 265º (this corresponds to waves propagating at an angle of 95º to the wavemaker and an angle of 65º to the normal to the breakwater). This can be seen in Fig. 6 with the estimated directional spectrum in front of the wavemaker for test 18.

Table 2 presents the wave characteristics obtained from the directional spectra estimated for the locations of the 3 arrays of acoustic wave probes. The column “Dir” contains the mean direction at the peak period. It can be seen in that table that the mean direction at the peak period in front of the wavemaker is almost 275º, which corresponds to the desired direction at the wavemaker.

Table 2. Wave characteristics. Quantities obtained from directional spectrum with IMLM.

| Test | Goal | | Array 3.3 | | | Array 3.2 | | | Array 3.1 | | |
|---|---|---|---|---|---|---|---|---|---|---|---|
| | Hs(m) | Tp(s) | Hs(m) | Tp(s) | Dir(º) | Hs(m) | Tp(s) | Dir(º) | Hs(m) | Tp(s) | Dir(º) |
| 17 | 0.100 | 1.19 | 0.108 | 1.21 | 276 | 0.108 | 1.19 | 274 | 0.107 | 1.21 | 274 |
| 18 | 0.150 | 1.45 | 0.151 | 1.46 | 276 | 0.159 | 1.46 | 276 | 0.152 | 1.46 | 270 |
| 19 | 0.175 | 1.57 | 0.169 | 1.59 | 276 | 0.171 | 1.58 | 269 | 0.171 | 1.58 | 272 |
| 20 | 0.200 | 1.68 | 0.190 | 1.71 | 275 | 0.183 | 1.70 | 270 | 0.178 | 1.70 | 274 |

As the sea state propagates towards the breakwater model, there are some changes in the mean direction at the peak period, although not larger than 7º. Close to the wavemaker, the trend observed in table 1 can also be seen: as the wave height goal increases, so does the difference between target and measurement. One may conclude that the wavemaker has some difficulty to generate the highest waves. By comparing the values in Table 1 and Table 2, one may conclude that the significant wave height obtained from the temporal analysis is quite similar to the one obtained from the directional spectrum.

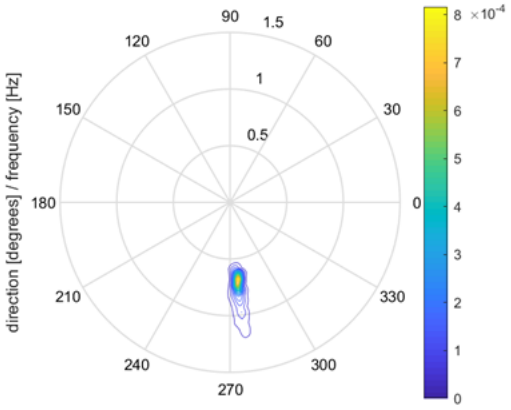


Figure 6. Directional spectrum estimated with the iterated maximum likelihood method. Data measured at the array of acoustic wave probes 3.3. Test 18: Hs = 0.150 m, Tp = 1.45 s.

One final test with the DIWASP toolbox was carried out with the free-surface elevation measured with the acoustic wave probe 3.2.6 (the central probe of array 3.2, the one in front of the breakwater head) and with the horizontal velocity components of the flow measured with ADV 2.3, the one closest to that acoustic wave probe. Since the ADV measurements did not start at the same time as the acoustic wave probes, the cross-correlation between the two signals was evaluated to find the time lag between them.
Fig. 7 presents the directional spectra obtained with such procedures for test 18 (Hs = 0.150 m Tp = 1.45 s). The agreement between the wave characteristics determined from the directional spectrum estimated from the probe + ADV data (Hs = 0.144 m Tp = 1,46 s Dir = 264º) with the ones from the spectrum estimated with the array data (Hs = 0.159 m Tp = 1,46 s Dir = 276º) is a foreseen consequence of the similar shapes of the directional spectra shown in that figure.

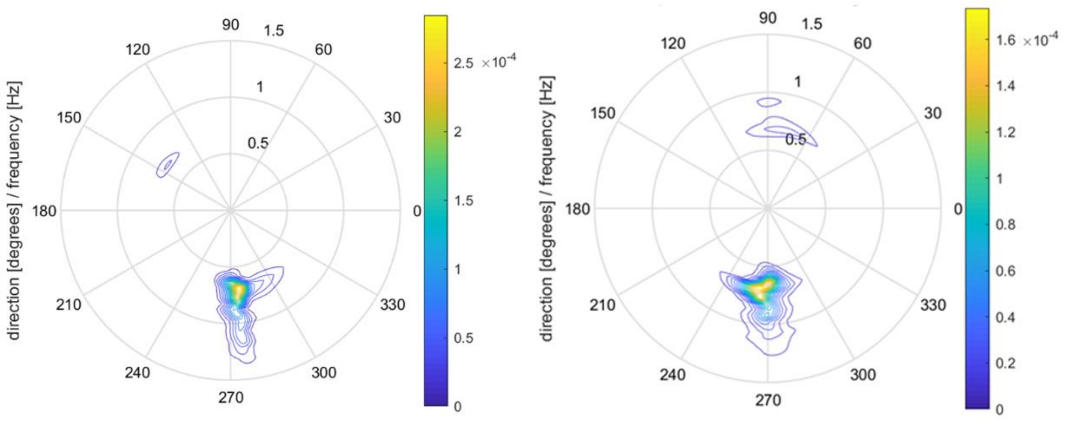


Figure 7. Directional spectra estimated with the iterated maximum likelihood method. Test 18: Hs = 0.15 m, Tp = 1.45 s. Left: data measured at the array of acoustic wave probes 3.3. Right: data measured at acoustic wave probe 3.2.6 and ADV 2.3.

## 5.2 Wave run-up and overtopping

Wave run-up and overtopping data analysis is still under progress.
Data from the capacitive gauges are used to determine the wave run-up height which is exceeded by 2 % of the incoming waves ($R_{2\%}$). The maximum wave run-up height for each run-up event is determined firstly. These values are than arranged with the highest first and the $R_{2\%}$ is determined. First attempts to analyse the video data led to the conclusion that this analysis will be very time consuming. The wave run-up on an armoured layer is characterised by a very turbulent and uneven water surface, which produces a lot of reflections. These reflections hinder a clear distinction of the upmost point of the water running up the slope. The use of different thresholds for converting the video frames into black-white pictures for data processing seems to be a promising way to overcome these difficulties.

## 5.3 Armour layer damage

A laser scan survey was carried out before the beginning of this set of tests (the second in a series of eleven) and before the eleventh set of tests. After each set of tests, the armour layer of the breakwater model had to be rebuilt, or at least some of the armour layer elements had to be put back in place. Before the last set of tests, the top layer of the armour with Antifer cubes (the breakwater roundhead and the adjoining trunk stretch 2.5 m wide) were completely rebuilt. Fig. 9 shows that despite all the rebuilding of the armour layer, no major differences were identified at one roundhead profile before the second set of tests and before the last set of tests.
Although photogrammetric data are still being processed, it is evident that the survey quality is highly dependent on the lighting conditions. Moreover, due to the rail height above the breakwater model, the surveyed area is limited to a strip 30 cm wide containing the still water level.
As to the Kinect surveys, preliminary results are quite interesting and innovative. In fact, to the authors' best knowledge, it is the first time that this sensor is used to measure damage in a breakwater head, with the sensor moving circularly along a rail.

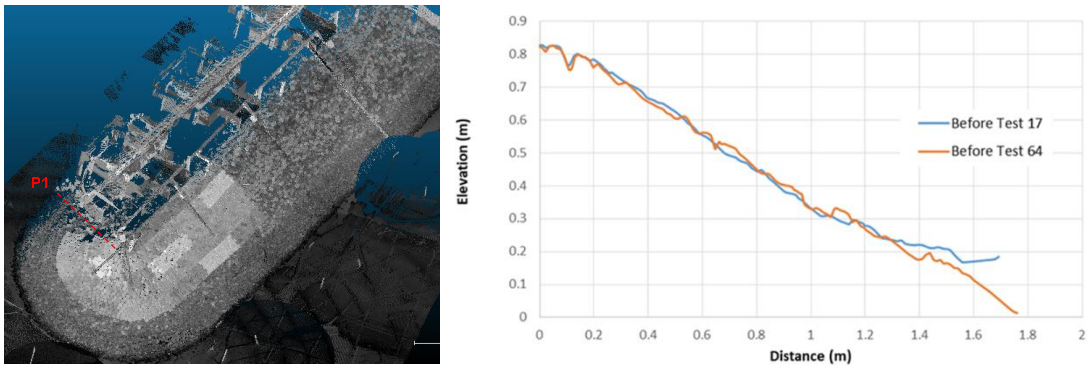


Figure 9. Roundhead profile at the beginning of the second and eleventh set of tests obtained from the laser scan survey.

The breakwater was correctly scanned, showing clearly the differences between the initial tests of the series with only movements between the armour units (increasing porosity) and tests with armour-unit extraction. Fig. 10 shows the initial state (before Test 17) and the final state (after Test 20) of the roundhead, whereas Fig. 11 presents the erosion and deposition data in mm. The density of area covered by the surface scanned was 0.50 points/mm$^2$. The analysis of the movements as a whole gave an estimation number of 19 pieces moved out of their initial position. The scanning results enabled the detection of minor movements between the Antifer cubes with a displacement equivalent to 3 units and the evolution of the local porosity going from the initial value of 0.296 to the final value of 0.303. These results do suggest that Kinect can be used by laboratories and research groups to identify the different damage stages with a good resolution, not only in 2D cases, but also in 3D studies.

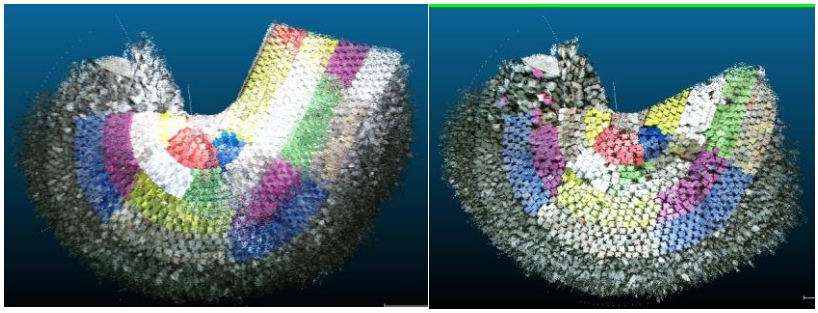

Figure 10. Roundhead scanned with Kinect. Left: before Test 17, Right: after Test 20.

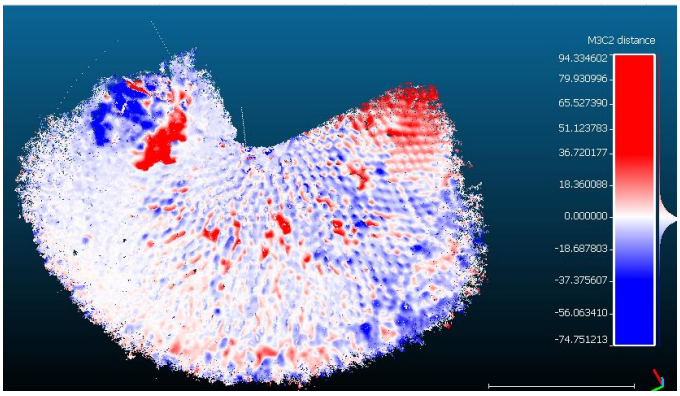


Figure 11. Movements of armour elements in the vertical direction. Red (erosion), blue (deposition.

For the Smartstone data, three approaches to detect the motions of Antifer cubes were tested:
(1) Local maxima above a certain threshold were obtained to calculate the number of peaks per number of waves. It was found that the obtained number of peaks per wave depends largely on the threshold and results in much higher numbers compared to values from the literature (e.g. Hofland et al., 2018).
(2) Cross-correlation of a defined reference event, representing a typical rocking situation that was manually selected from the Smartstone data, resulting in a number of events per number of waves. Event detection based on correlation showed generally large differences to the visual

estimation of the number of events, both in terms of the number and the temporal localization. The correlation technique appears to be more effective for gyroscope data, compared to the application for accelerometer data.
(3) A combination of high-pass and low-pass filters was applied and combined with a threshold also resulting in a number of events per number of waves. Events based on filtering were closest to the visual interpretation, but they were also influenced by the filter parameters.
The Arduino type smart Antifers did give signals over the duration of the test. A sampling frequency of 25 Hz could be obtained. This seems to be enough to obtain the rotational velocities directly from the gyroscopes. However, for obtaining the translation movements from integration of the accelerometer signals, this seemed to be insufficient.
Fig. 12 presents the recording of the motions of Cube 3 in test 29 (same water depth, long-crested waves with incidence angle of 40º, Hs = 0.175 m and Tp = 1.57 s). Cube 3 was one of the cubes that functioned during all tests. At the location of Cube 3 the regular packing of the Antifers opened up a little during testing. Moreover, the wave velocities are high. Hence, motion and rocking of the units can be expected. The location of Cube 3 before and after the test is indicated in Fig. 5. Cube 3 can be seen to have shifted during the test. In the top left graph of Fig. 12 the distribution over its components of the steady gravitational acceleration of 1G upward, can be seen to have shifted around t = 700 s. Hence, the cube's orientation relative to the horizontal plane has changed. Fig. 12 shows that Cube 3 rocked for nearly every wave, also around 700 s. As only one or two measurements are made during a rocking event, the accelerometer cannot be used to obtain a reliable estimate of the translation impact velocity, as that requires integration. As the gyroscope measured directly the rotational velocity θ, this rotational impact velocity is somewhat more reliable, and can be used for the structural analysis of the concrete Antifers. Since other cubes showed much less movement, this means that many cubes will have to be instrumented to obtain a good idea about the rocking motion of the entire armour layer. Hence it is of paramount importance that any such measurement technique is affordable.

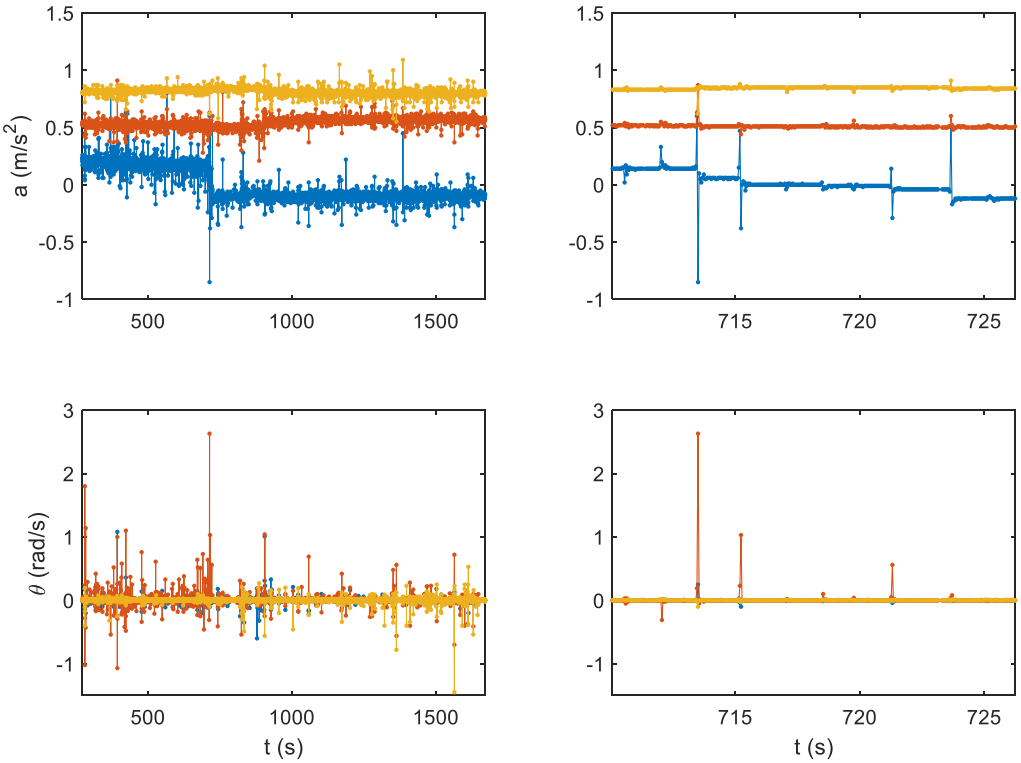


Figure 8. Time series of linear accelerations and angular velocities measured by Cube 3 in test 28.

## 6. CONCLUSIONS

The RODBreak experiment was a unique opportunity to characterize the influence of wave incidence obliquity on run-up, overtopping and damage evolution of the armour layer of rubble-mound breakwaters.

The incident waves produced by the wavemaker did comply with the plan, which means that the intended steepness of 0.055 was achieved.
This experiment also enabled the testing of several measuring procedures for armour layer evolution.
The two laser scan surveys before the beginning of the second and eleventh test series showed that, despite the wave action and the armour layer reconstructions, there was no significant settling of the breakwater model.
Although there is still a lot to process in the photogrammetry and Kinect surveys, it is clear that the results from the surveys of the armour layer envelope are relevant to understand the first stages and behaviour of the roundhead evolution, and to develop maintenance strategies before damage reaches failure.
The most effective technique to detect the motions from the Smartstone (Antifer cubes) data appears to be a filter-based technique applied to gyroscope data. Exemplary analysis of influencing factors for motions showed a generally higher number of events or peaks per waves for larger wave heights and positions close to the water level. However, these differences were mostly not significant.
The Arduino-based smart Antifer devices proved rather robust in use, although the sampling frequency needs to be increased. The number of impacts between Antifers (potentially leading to mechanical fracturing) and the extreme rotational velocities could be obtained.

## ACKNOWLEDGEMENTS

This project has received funding from the European Union's Horizon 2020 research and innovation programme under grant agreement No 654110, HYDRALAB+.
The authors would like to acknowledge the support from the Ludwig-Franzius Institute (LuFI), namely from Dr.-Ing. Sven Liebisch and specially the people at Marienwerder: Björn, Mareike, Mario, Raoul and Tom.

## REFERENCES

Bornschein, A., Pohl, R., Wolf, V., Schüttrumpf, H., Scheres, B., Troch, P., Riha, J., Spano, M. and Van der Meer, J. (2014). Wave run-up and wave overtopping under very oblique wave attack (CORNERDIKE-project). Proc. HYDRALAB IV Joint User Meeting, Lisbon, July.

Gronz, O., Hiller, P.H., Wirtz, S. and Ries, J.B. (2016) Smartstones: A small 9-axis sensor implanted in stones to track their movements, Catena, 142, 245-251.

Hofland, B., Arefin, S.S., Van der Lem, C. and Van Gent, M.R.A. (2018) Smart rocking armour units. Proc. 7th Int. Conf. on the Application of Physical Modelling in Coastal and Port Engineering and Science (Coastlab18), Santander.

Hofland, B. and Van Gent, M.R.A. (2016) Automatic settlement analysis of single-layer armour layers. Proc. 6th Int. Conf. on the Application of Physical Modelling in Coastal and Port Engineering and Science (Coastlab16), Ottawa.

Johnson, D. (2002) DIWASP, a directional wave spectra toolbox for MATLAB®: User Manual. Research Report WP-1601-DJ, Centre for Water Research, University of Western Australia.

Nørgaard, J.Q.H., Lykke Andersen, T., Burcharth, H.F. and Steendam, G.J. (2013) Analysis of overtopping flow on sea dikes in oblique and short-crested waves, Coast. Eng. 76, 43–54.

Pawka, S.S. (1983) Island shadows in wave directional spectra, J. Geophys. Research, 88(C4), 2579-2591.

Pedro, F., Bastos, M., Lemos, R., Fortes, C. and Santos, J.A. (2015) Toe berm damage progression analysis using a stereophotogrammetric survey technique, Proc. 7th SCACR - Int. Short Course/Conf. on Applied Coastal Research, Florence.

Sande, J., Laiño, E., Peña, J., Neves, M.G., Lemos, R., Figuero, A., Reis, M.T., Alvarellos, A. and Rabuñal, J. Application of scanning techniques for damage analysis in rubble mound breakwaters. Proc. 7th International Conference on the Application of Physical Modelling in Coastal and Port Engineering and Science (Coastlab18), Santander.

Van Gent, M.R.A. (2014) Oblique wave attack on rubble mound breakwaters, Coast. Eng. 88, 43-54.